Asociación Argentina
de Mecánica Computacional

Mecánica Computacional Vol XXXIII, págs. 2185-2199 (artículo completo)
Graciela Bertolino, Mariano Cantero, Mario Storti y Federico Teruel (Eds.)
San Carlos de Bariloche, 23-26 Setiembre 2014

EVALUATION OF PIEZOELECTRIC ENERGY HARVESTING FROM SUPERIOR MODES

Sebastián P. Machado[a], **Mariano Febbo**[b] **and S. Bellizzi** [c]

[a]*Grupo de Análisis de sistemas mecánicos, Centro de Investigaciones de Mecánica Teórica y Aplicada, Universidad Tecnológica Nacional FRBB, 11 de Abril 461, 8000 Bahía Blanca, Buenos Aires, Argentina*

[b]*Instituto de Física del Sur y Departamento de Física, Universidad Nacional del Sur, Avda. Alem 1253, 8000 Bahía Blanca, Buenos Aires, Argentina, mfebbo@uns.edu.ar http://www.uns.edu.ar*

[c]*LMA, CNRS, UPR 7051, Aix-Marseille Univ, Centrale Marseille, F-13402 Marseille Cedex 20, France*

Keywords: Piezoelectric energy harvesting, superior modes, base excitations.

Abstract. In this work we present the analytical model and experimental results of a vibration energy harvesting device with a PZT piezoceramic sheet under vibration-based excitation. The voltage and electric power generation is presented for the first two modes and compared. Also, the consideration of a tip mass to improve the energy generation is discussed for the considered cases. Finally, some conclusions remarks are drawn which show the benefits and possible disadvantages of generating power for high frequencies.

1 INTRODUCTION

Piezoelectricity is the property of certain materials to exhibit electric polarization proportional to the applied strain (direct effect). It was first discovered in 1880 by French brothers Jacques and Pierre Curie (1). The converse is also true, this means, these materials become strained when they are subjected to an electric polarization (inverse effect). Several natural materials such as quartz, topaz and Rochelle salt, for example, were observed to show the piezoelectric effect. Most striking are the cases of biological matter such as DNA and the recently discovered M13 bacteriophage virus (2) that can display piezoelectric properties. With the progress of materials science in the second half of last century, the discover of new piezoelectric ceramics permit to build materials with a large electromechanical coupling between the mechanical and electrical behaviors. At the same time, small electronic components of wireless sensors and wearable electronics require low electric power to work. Under these circumstances, the researchers have begun to develop vibration-based piezoelectric harvesters to supply the energy, extend the life and reduce the volume of the electronics, obtaining electrical energy from the ambient energy surrounding the device (3). From an ecological viewpoint the possibility of replacing batteries using these energy harvesters entails a reduction of the contaminated solid waste coming from the batteries.

Piezoelectric energy harvesting is only one possibility among others of harvesting energy from various ambient sources, including solar power, thermal gradients, nuclear reactions and so on (4). Its fundamental advantage lies in they have high electromechanical coupling which means a large strain/voltage conversion, require no external voltage source and are adequate to miniaturize (5), (6), (7).

The aim of the present work is to analyze the power generation of a vibration-based excited system considering superior modes of vibration of a cantilever beam with an attached piezoelectric ceramic layer.

After an introductory section, section 2 introduces the mathematical formulation of the problem. The following section 3, presents the results concerning the generation of voltage and power of the piezoelectric beam as a function of the frequency of excitation. The consideration of a mass added at the end of the beam to improve the generation, will also be studied and analyzed for the whole range of considered frequencies. Concluding remarks are then presented and discussed in section 4.

2 MATHEMATICAL DESCRIPTION AND MODELLING

The system under study comprises a PZT-5A piezoceramic layer (QP16N, Midé Corporation) attached to a beam as can be seen in Fig. 1 (a). The system undergoes base excitation over the form of a deterministic function $g(t)$ or electromagnetic excitation under an harmonic force of the form $f\cos(\omega t)$ at $x = x_f$. Both ways of excitation try to mimic an environmental excitation from which energy can be extracted.

Now, we wish to review the derivation of the relationships between the electric and mechanical variables as can be found in (8). The first law of thermodynamics (the principle of conservation of energy) for a linear piezoelectric continuum leads to (9)

$$\dot{U} = T_{ij}\dot{S}_{ij} + E_i\dot{D}_i \tag{1}$$

where U is the stored energy density of the piezoelectric continuum, T_{ij} is the stress tensor, S_{ij} is the strain tensor, E_i is the electric field, D_i is the electric displacement and the overdot represent differentiation with respect to time, as usual. The electric enthalpy density H is given

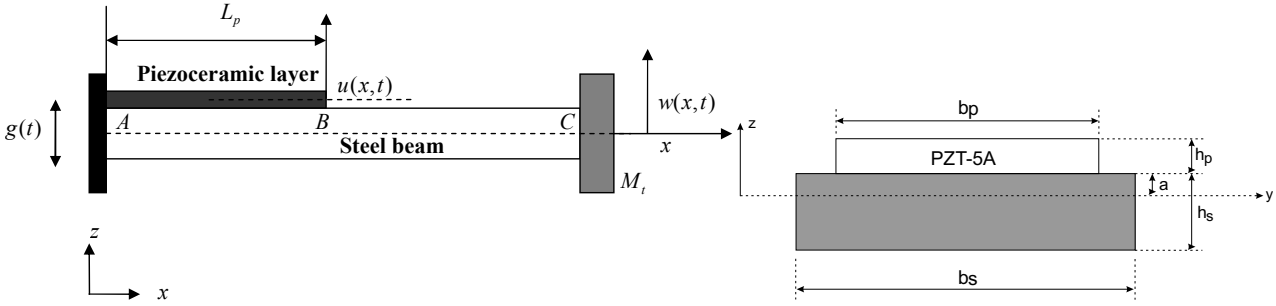

Figure 1: (a) Schematic illustration of a piezoelectric layer attached to a steel beam. (b) Cross sectional view of the electromechanical system.

by

$$H = U - E_i D_i \tag{2}$$

Substituting Eq. (1) into Eq. (2) results

$$\dot{H} = T_{ij}\dot{S}_{ij} - D_i\dot{E}_i \tag{3}$$

which means that enthalpy is a function of the stress tensor and the electric field in the form of $H = H(S_{ij}, E_i)$ so that the components of the stress and the electric displacement tensors can be derived from the electric enthalpy density as

$$T_{ij} = \frac{\partial H}{\partial S_{ij}}, \qquad D_i = -\frac{\partial H}{\partial E_i} \tag{4}$$

The form of the electric enthalpy density in the linearized theory of piezoelectricity is (8)

$$H = \frac{1}{2}c^E_{ijkl}S_{ij}S_{kl} - e_{kij}E_kS_{ij} - \frac{1}{2}\varepsilon^S_{ij}E_iE_j \tag{5}$$

where c^E_{ijkl}, e_{kij}, and ε^S_{ij} are the elastic, piezoelectric, and permittivity constants, respectively, while the superscripts E and S denote that the respective constants are evaluated at constant electric field and constant strain, respectively. Now, we use Eqs. (4) and (5) along with the relation $\partial S_{ij}/\partial S_{ji} = \delta_{ij}$ due to the symmetry of the stress tensor (where δ_{ij} is the Kronecker delta) to obtain and expression for the stress tensor

$$T_{ij} = c^E_{ijkl}S_{kl} - e_{kij}E_k \tag{6}$$

and for the electric displacement vector

$$D_i = e_{ikl}S_{kl} + \varepsilon^S_{ik}E_k \tag{7}$$

which represent the linear constitutive equations for the unbounded piezoelectric continuum and are the relations which will be used in the following derivations.

To derive the equations for the displacement field of the system and the voltage output of the piezoelectric layer, we use a Lagrangian approach. As can be seen in Fig. 1 (a) the system comprises a piezoceramic layer (hereafter piezo) bonded over a steel beam (hereafter beam). The kinetic energy for the piezo is then:

$$T_p = \frac{1}{2}\rho_p A_p \int_0^{L_p} (\dot{w}(x,t) + \dot{g}(t))^2 dx \tag{8}$$

and for the beam

$$T_b = \frac{1}{2}\rho_b A_b \int_0^{L_b} (\dot{w}(x,t) + \dot{g}(t))^2 dx \tag{9}$$

where L_p is the length of the electrically active piezoceramic material, L_b is the length of the steel beam, $w(x,t)$ is the spatio-temporal transverse deflection, $g(t)$ is the base displacement ρ_p and ρ_b are the piezo and beam material density, and A_p and A_s are the cross-sectional area of the piezo and beam respectively. Additionally the kinetic energy of the end mass or tip mass m_T can be computed as

$$T_m = \frac{1}{2} m_T (\dot{w}(x,t) + \dot{g}(t))^2 \tag{10}$$

where the rotational inertia of the tip mass has been neglected. To compute the potential energy the beam only store energy in the form of elastic linear potential energy. We employ Euler-Bernoulli theory to this end which states that the linear inextensible strain through the beam is a result of bending motion only (first term in right hand member of Eq. (3) and proportional to the second spatial derivative of the bending coordinate, i.e. $S_{11} = S_x = -zw''(x,t)$ where $()'$ means $\partial/\partial x$. Finally the integral expression of the elastic linear potential energy of the beam, after integrating over the $y-$ and $z-$ directions gives

$$U_b = \frac{1}{2} E_b I_b \int_0^{L_b} (\dot{w}(x,t))^2 dx \tag{11}$$

where E_b is Young's modulus for the beam and $I_b = bh_b^3/12$ its mass moment of inertia. For the piezo, the expression for the enthalpy has been calculated in Eq. (5) and comes from the mechanical bending of the laminate and from the electric field due to the applied strain. Finally, the integral expression for the bending enthalpy is:

$$H_p = \frac{1}{2} \int_{V_p} [z^2 E_p (w''(x,t))^2 + 2z e_{zx} E_z(t)(w(x,t)'' - \varepsilon_{zz}^S E_z(t)^2] dV_p \tag{12}$$

where V_p is the volume of the piezo layer, $c_{1111}^E = E_p$ is the Young's modulus for the piezoelectric material and E_z is the electric field in the z direction. In order to continue with the derivation of the equations, the electric field in the piezo layer is assumed to be uniform through the thickness of the laminate similar to a capacitor. In the electrical field a common choice is to select the voltage output as the generalized or independent coordinate (10). In this case, following Stanton *et.al.* (11) we choose the flux linkage (canonical conjugate of the charge $q(t)$) as the generalized coordinate. Then, the electric field in the piezo may be written as:

$$E_z(t) = -\dot{\lambda}(t)/2h_p \tag{13}$$

where h_p is the laminate thickness and the time derivative of flux linkage λ has units of Weber per second or Volts. An schematic view of the cross-sectional area of the electromechanical system is plotted in Fig. 1 (b). Inserting Eq.(13) into Eq.(11) and integrating in the $y-$ and $z-$ directions gives

$$H_p = E_p I_p \int_0^{L_p} (w''(x,t))^2 dx - \frac{1}{2} e_{zx} b(h_p + h_b)\dot{\lambda}(t) w'(L_p,t) - \frac{1}{4} C_p \dot{\lambda}(t)^2 \tag{14}$$

where the piezo moment of inertia is given by $I_p = bh_p(4h_p^2 + 6h_p h_b + 3h_b^2)/12$ (see appendix),the capacitance is $C_p = b\varepsilon_{zz}^S L_p/h_p$ and $e_{zx} = d_{31} c_{11}^E$ where d_{31} is the piezoelectric constant

and c_{11}^E is the Young modulus of the piezoceramic layer. The Lagrangian functional for the electromechanical system is then given by:

$$\mathcal{L}(w,\dot{\lambda}) = T_b + T_p + T_{m_T} - U_b - H_p \tag{15}$$

Then, the equations of motion are obtained by using Hamilton's principle. However, it is possible to obtain the equations of motion in a more direct way. By using a modal expansion of the displacement field $w(x,t)$, it is possible to write a Lagrangian in some group of time-dependent generalized modal coordinates. Then, after applying Euler-Lagrange equations, a set of ordinary differential equations may be obtained.

2.1 Modal expansion

We assume that the displacement field of the system can be written as a sum of N time-dependent generalized modal coordinates and orthogonal modes of the form

$$w(x,t) = \sum_{j=1}^{N} \eta_j(t)\phi_j(x). \tag{16}$$

Considering the case under study, the system can be viewed as two separate Euler-Bernoulli beams one after the other. In this sense, the modes of the system have to take into account the effect of this union. For the sake of brevity, we refer the reader to the appendix for a better explanation of the mathematical procedure to obtain $\phi_j(x)$.

2.2 Final expressions for the electromechanical system

Now, using the $\phi_j(x)$ Eq. (15) can be calculated. Finally, it is

$$\mathcal{L}(\eta,\dot{\eta},\dot{\lambda}) = \sum_{j=1}^{N} \frac{1}{2}[\dot{\eta}_j(t)^2 + m\dot{g}^2(t)] - \frac{1}{2}\omega_j^2\eta_j(t)^2 + \theta_j\dot{\lambda}(t)\eta_j(t) + \frac{1}{4}C_p\dot{\lambda}^2(t) + \Gamma_j\dot{\eta}_j(t)\dot{g}(t) \tag{17}$$

where $m = \rho_s A_s L_b + 2\rho_p A_p L_p$ is the total mass of the system (without the tip mass) and ω_j are the total beam natural frequencies, the electromechanical coupling term is:

$$\theta_j = \frac{e_{zx}}{2} b_p \frac{(ah_p + \frac{h_p^2}{2})}{h_p} \phi_j'(L_1) \tag{18}$$

and Γ_j is the modal coupling given by:

$$\Gamma_j = \rho_1 A_1 \int_0^{L_1} \Phi_{j,1} dx + \rho_2 A_2 \int_{L_1}^{L_1+L_2} \Phi_{j,2} dx \tag{19}$$

where $\Phi_{j,k}$, $k = 1, 2$, L_1 and L_2 are given in the appendix.

From this moment, we only consider one mode. Now, we apply the Euler-Lagrange equations to Eq. (17)

$$\frac{d}{dt}\left(\frac{\partial L}{\partial \dot{\eta}}\right) - \frac{\partial L}{\partial \eta} = Q(t) \tag{20}$$

and

$$\frac{d}{dt}\left(\frac{\partial L}{\partial \dot{\lambda}}\right) - \frac{\partial L}{\partial \lambda} = I(t) \tag{21}$$

where $Q(t)$ represents a generalized force and $I(t)$ is a generalized current. From the theory of electric circuits it must be recall that the generalized current represents the rate of change in flux linkage through the energy harvesting network, represented by an equivalent resistive load, i. e. $I(t) = -\dot{\lambda}(t)/R_L$. Finally, by applying Eqs. (20) and (21) we have:

$$\ddot{\eta}_j + 2\xi_j\omega_j\dot{\eta}_j + \omega_j^2\eta_j - \theta\dot{\lambda} = \Gamma_j\ddot{g} \tag{22}$$

and

$$C_p\ddot{\lambda} + \frac{1}{R_l}\dot{\lambda} + \theta_j\eta_j = 0 \tag{23}$$

Now, introducing the voltage $v(t) = -\dot{\lambda}(t)$ and assuming an harmonic dependence of all variables ($v(t) = \overline{v}e^{i\Omega t}$ and $\eta(t) = \overline{\eta}e^{i\Omega t}$) we arrive, after applying the harmonic balance method (12) at the equations for the voltage

$$\overline{v} = \frac{\Gamma_j\theta\Omega R_l}{\sqrt{(\omega_j^2 - \Omega^2 - 2C_pR_l\xi_j\omega_j\Omega^2)^2 + (2\Omega\xi_j\omega_j + R\Omega(\theta_j^2 + C_p\omega_j^2 - C_p\Omega^2))^2}} \tag{24}$$

and for the modal coordinate

$$\overline{\eta} = \frac{\Gamma_j\sqrt{1 + C_p^2R_l^2\Omega}}{\sqrt{(\omega_j^2 - \Omega^2 - 2C_pR_l\xi_j\omega_j\Omega^2)^2 + (2\Omega\xi_j\omega_j + R\Omega(\theta_j^2 + C_p\omega_j^2 - C_p\Omega^2))^2}} \tag{25}$$

To obtain the displacement field for frequencies near mode j, we must evaluate $w(x,t) = \sum_{k=1}^{2}\phi_{j,k}\overline{\eta}_j\ e^{i\Omega t}$

3 EXPERIMENTS AND DISCUSSION

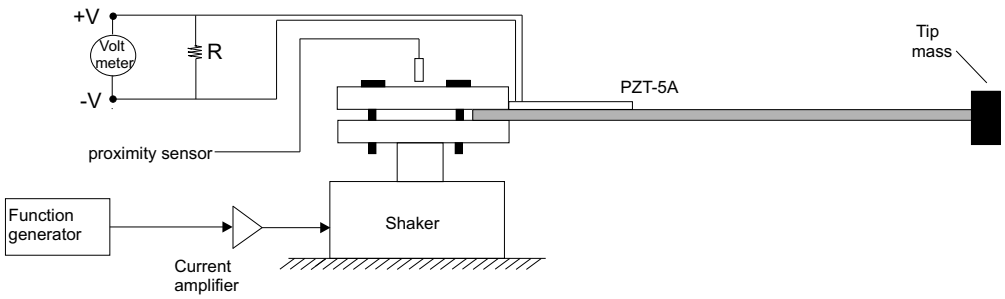

Figure 2: Connection diagram of the experimental setup.

In this section we present the experimental results and its comparison between the numerical calculations provided by the analytical model. In the experiments, the excitation is provided by a shaker. Base displacement is measured by a displacement proximity sensor and then converted into acceleration. The sinusoidal excitation is provided by a signal generator in a frequency sweep over the frequencies of interest and its power adjusted by a power amplifier. All measured signals are then recovered into the correct format for postprocessing using a data acquisition system. An schematic view of the connection diagram of the experimental setup can be observed in Fig. (2). The actual setup for the experiment is illustrated in Fig. (3).

In Table (1) we present the physical and geometrical parameters of the steel beam and of the piezoceramic layer (QP16N, Midé Corporation)

Table 1: Geometrical and physical parameters of the prototype device consisting in a steel beam and a piezoelectric beam used for the experiments

Geometrical parameters	beam (steel)	piezoelectric layer (PZT)	Material parameters	beam	piezoelectric layer
Length, L (mm)	137	45.9	density ρ (kgm^{-3})	7800	7800
width, b (mm)	31.8	20.57	Young modulus, E (GPa)	210	67
thickness, b (mm)	0.9	0.25	piezo constant, d_{31} (pm V^{-1})	—	-190
mass M_t, (kg)	–	–	permittivity ϵ_{33}^S (pFm^{-1})	—	1500 ϵ_0

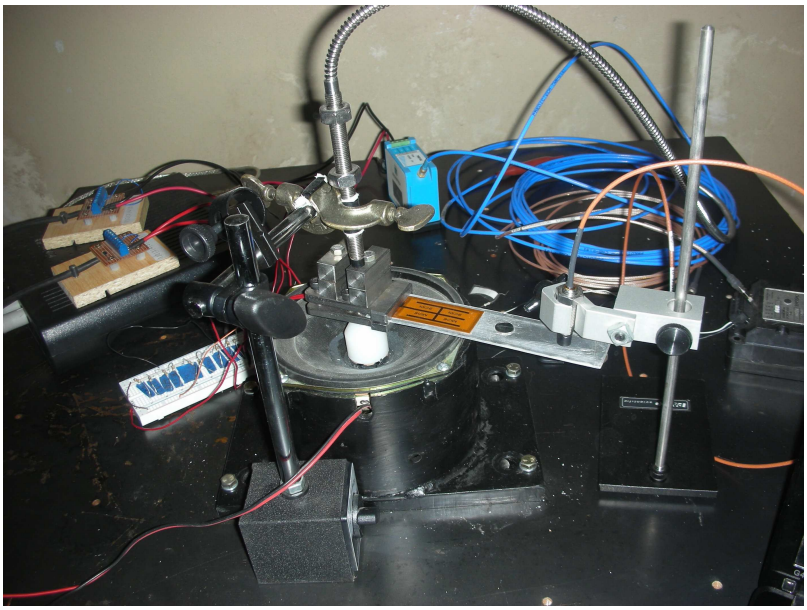

Figure 3: Experimental setup for the proposed system.

In the following, the experimental results are presented for the first two modes with the addition or not of a point mass at the end of the vibrating system. The motivation of this is to elucidate the effect of the addition of mass for the superior modes in the generation of energy compared with the fundamental mode of vibration.

Now, we analyze the system which is excited by a base displacement through an electromagnetic shaker. The results of the voltage frequency response function FRF is compared then with Eq. (24).

It should also be added that the FRFs in Eq. (24) are multiplied by $g = 9.81m/s^2$ which is the preferable standard (see for example (10)). It is usual to present the results for different values of the resistive load. This situation try to emulate different load conditions as it is common in real applications. Additionally, the effective load resistance observed across the electrodes of the harvester is the equivalent resistance of the resistive load used and $R = 984\text{k}\Omega$, which is the input resistance of the data acquisition system. The electrical connection imposes that they see

each other in parallel so, the effective load resistance is: $R_e = 1/(1/R_l + 1/R_{ad})$ whose values are presented in Table (2).

The voltage and power FRFs for the first mode are presented in Figs. (4) and (5) with $m_T = 0$ (no addition of mass). The damping coefficient of the first mode was set to $\xi_1 = 0.02$ to best fit the voltage for the large resistive load.

Table 2: Effective load resistance which is the parallel between the used (measured) resistance and $R = 986k\Omega$ (input resistance of the data acquisition system).

R_l(measured)	R_e(effective)
-	986 kΩ $(986 \times 10^3\Omega)$
326 kΩ	244 kΩ
98.3 kΩ	89.4 kΩ
32.7 kΩ	31.6 kΩ
9.92 kΩ	9.82 kΩ
0.984 kΩ	0.983 kΩ

Figure (4) shows the voltage generation in the nearness of the first mode of the system for the whole set of considered resistances. There, it can be observed a perfect agreement between the theoretical (numerical) and experimental results. The maximum value of $\mathrm{V/g}$ is $\sim 18.5\mathrm{V/g}$ and is for the maximum load resistance. The minimum, instead, is on the order of $1\mathrm{V/g}$ and is for the lowest resistance which is the case of the more current consuming.

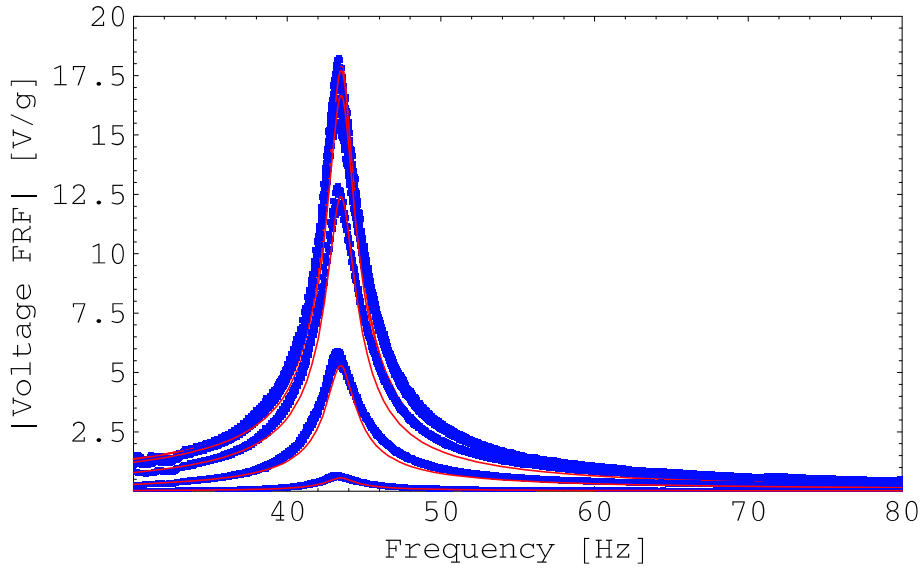

Figure 4: FRFs for frequencies near the first mode of the piezoelectric beam for a given set of resistors. The electromechanical beam has no addition of mass and the system is base-excited. Solid lines theoretical, circles experimental.

In agreement with other previous results (10), the maximum generation (peak) moves slightly to lower frequencies for lower resistances since the resistance R_l can be viewed as an effective (although electrical) damping. At the same time, the electrical power generated can be observed in Fig. (5). There, the different curves show the electrical power for the whole set of resistances. The maximum generated power is for resistance $R_l = 32.7\mathrm{k}\Omega$ and it is $5\mathrm{mW}$. The comparison

with the other experimental results are not shown here, for a better presentation of the curves. However, a similar agreement is observed.

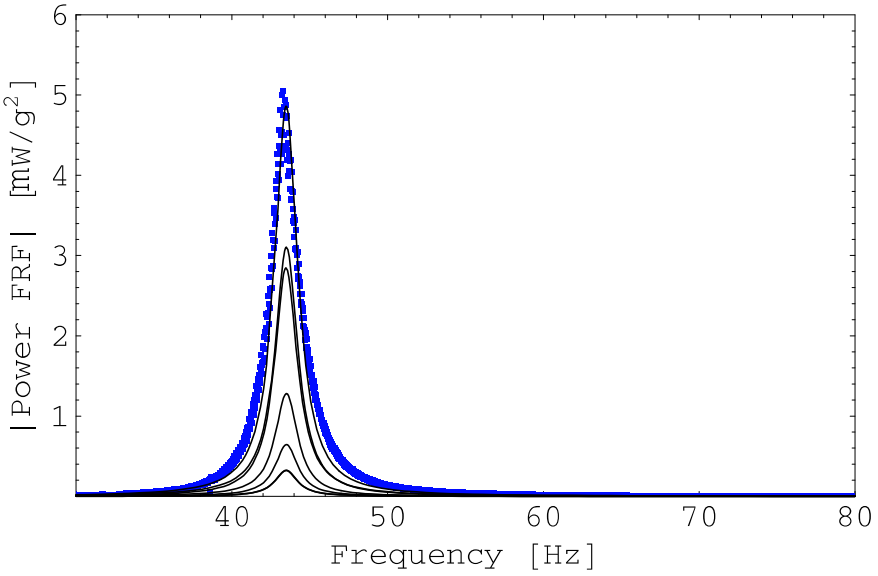

Figure 5: Generated electrical power for frequencies near the first mode of the piezolectric beam of Fig. 4. Solid lines theoretical, circles experimental.

Figure (6) shows the voltage generation with a small addition of mass, which was selected to be of $m_T = 2.41\text{gr}$. The first salient feature is that the overall generation of voltage increases from $\sim 18.5V/g$ to $\sim 23V/g$ which represents almost a 25% of increment. Also, the addition of mass causes the system to lower its resonant frequency for the whole considered cases.

Additionally, the generated power is shown in Fig.(7) and has maximum value of 6.8mW for $R_l = 32.7\text{k}\Omega$. This power represents an increment of 36% with respect with the case of no addition of mass.

Now, we present the results for frequencies near the second mode of the beam system. The generated voltage and power are shown in Fig. (8) and (9) with no addition of mass. It is first noted that the voltage generation in these frequencies is reduced in magnitude. In this case, we have a maximum generated voltage of $\sim 5.2V/g$ which is more than three times lower than the voltage generated for frequencies near the first mode. As a consequence, a similar tendency is followed by the generated electrical power. The results for the power in Fig. (9) reveals that this value is more than four times lower than the case involving the first mode.

The addition of mass in this case is considered in Fig. (10). For a meaningful comparison, we have added the same mass as for the case of frequencies near the first mode. The generated output voltage for the maximum resistance is 7.5 V/g in this case. This represents an increment of almost 45 $\%$ compared with the voltage generation in the absence of mass. Consequently, this increment is reflected in the generated power shown in Fig. (11). In absolute terms, this power is approximately 3.6 mW which, compared with 6.8mW with the same case for frequencies near the first mode represents a decrement of only 50 $\%$.

A comparison of the maximum voltage and maximum power generation as a function of frequency is shown in Fig. (12). There, it is possible to observe the effect of the addition of mass in the generation of voltage (or power) relative to the maximum voltage (or maximum power) which happens for the first mode with added mass. If we analyze the power, it is possible to

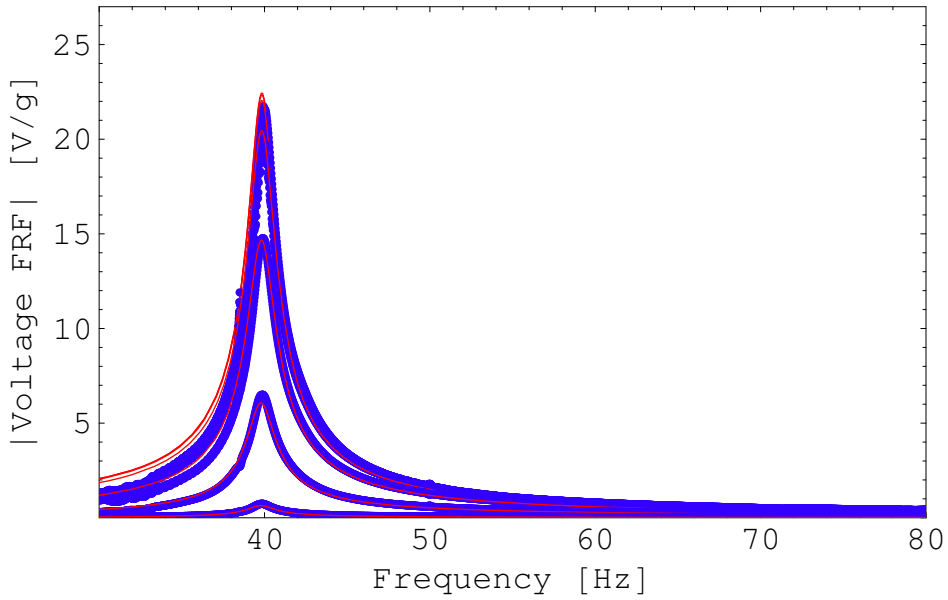

Figure 6: FRFs for frequencies near the first mode of the piezoelectric beam for a given set of resistors. A tip mass is considered in this case and the system is base-excited. Solid lines theoretical, circles experimental.

observe a large separation for the second mode between the cases with mass and without mass, compared with the same case for the first mode. Instead, this situation is reversed if we analyze the voltage.

4 CONCLUSIONS

In this work we analyze the effect in the generation of energy of superior modes of vibration. From the considered cases, it is possible to draw the following conclusions

- Voltage generation presents a maximum for frequencies in the nearness of the first mode of vibration.
- It is possible to improve the voltage and power generation with an addition of mass at the end of the piezoelectric beam.
- The maximum power generation is for a value of load resistance which is not the same which maximizes the voltage
- The difference between the maximum generated power with or without the consideration of mass is more pronounced for high frequencies. The opposite occurs for the maximum voltage generation.
- In absolute terms, the generated power for the second mode with the addition of mass is only 30 % lower compared with the first mode without the addition of mass.

ACKNOWLEDGEMENTS

S. P. Machado acknowledges CONICET and Secretaría de Ciencia y Tecnología UTN FRBB. M. Febbo acknowledges CONICET and Secretaría de Ciencia y Tecnología UNS.

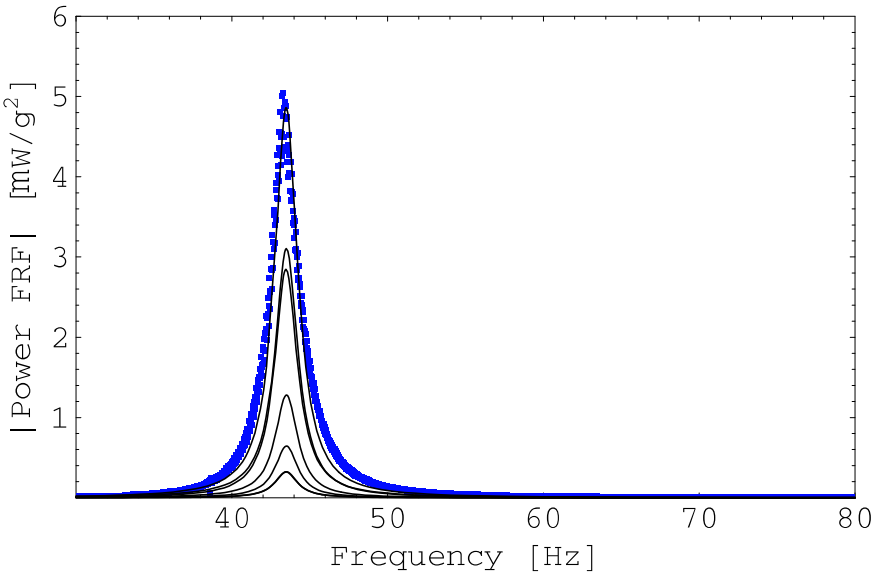

Figure 7: Generated electrical power for frequencies near the first mode of the piezolectric beam of Fig. (6). Solid lines theoretical, circles experimental.

APPENDIX. DERIVATION OF NON-UNIFORM MODES FOR THE COMPOSE SYSTEM

The system under analysis comprises a piezoelectric layer bonded over the top of a beam. In this sense, the system can be treated as a compose system. In this section we concentrate on calculating the non-uniform mode that result from this compose system. Allowing for an artificial break at $x = L_p$, the total beam is assumed to be as two separate Euler-Bernoulli beams satisfying continuity and compatibility conditions at its junction.
Thus, the mode shapes for the beam can be written as:

$$\phi_j(x) = \sum_{k=1}^{2} \Phi_{j,k}(x) H_k(x) \tag{26}$$

where k is the number of sections and $H_k(x)$ is the Heaviside function to denote the break at $x = L_p$. Here, 1 stands for first the section $A - B$ and 2 for the second section $B - C$ (for clearness refer to Fig. 1)) Therefore $L_1 = L_p$ and $L_2 = L_b - L_p$. Then, $\Phi_{j,1}$ results, considering the piezoelectric laminate:

$$\Phi_{j,1}(x) = C_1 \sin(\beta_{j,1}x) + C_2 \cos(\beta_{j,1}x) + C_3 \sinh(\beta_{j,1}x) + C_4 \cosh(\beta_{j,1}x) \tag{27}$$

where C_i represent constants determined by the boundary conditions and $\beta_{j,1}$ are the eigenvalues given by $\beta_{j,1}^4 = \omega^2 \rho_1 A_1/(E_1 I_1)$. The $(A - B)$ beam sectional properties are given by integrating $1/2 \int_S z^2 E dy dz$ over the cross sectional area S. This gives:

$$E_1 I_1 = \frac{1}{12} b_s E_s h_s^3 + 2 b_p E_p \left(\frac{h_p^3}{3} + \frac{h_p^2 h_s}{2} + \frac{h_p h_s^2}{4} \right) \tag{28}$$

$$\rho_1 A_1 = 2 b_p h_p \rho_p + b_s h_s \rho_s \tag{29}$$

For the second section $B - C$ the solution is:

$$\Phi_{j,2}(x) = C_5 \sin(\beta_{j,2}x) + C_6 \cos(\beta_{j,2}x) + C_7 \sinh(\beta_{j,2}x) + C_8 \cosh(\beta_{j,2}x) \tag{30}$$

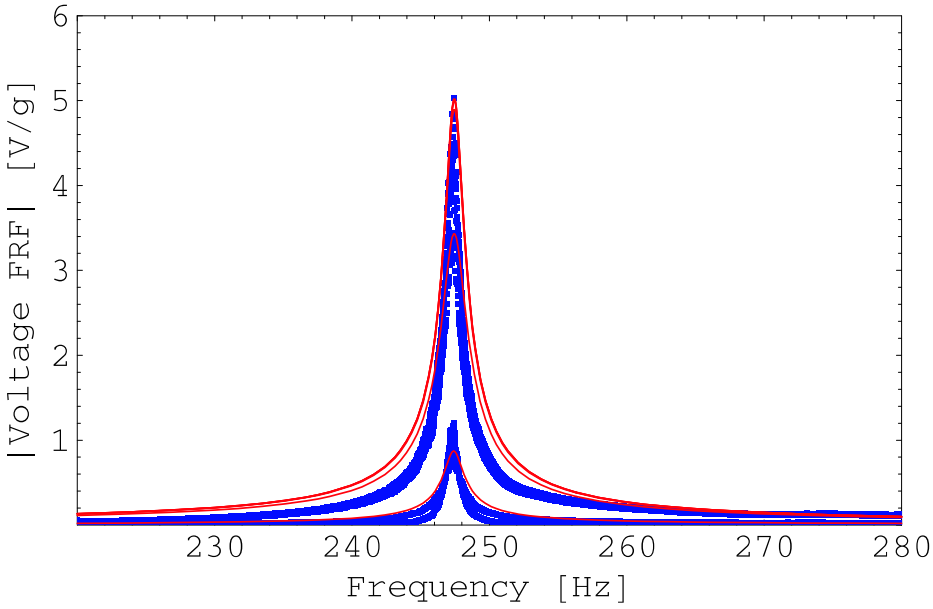

Figure 8: FRFs for frequencies near the second mode of the piezoelectric beam for a given set of resistors. The electromechanical beam has no addition of mass and the system is base-excited. Solid lines theoretical, circles experimental.

and C_{5-8} are determined by boundary conditions. In this case, the eigenvalues are $\beta_{j,2}^4 = \omega^2 \rho_2 A_2/(E_2 I_2)$. Similarly, the sectional properties are given by

$$E_2 I_2 = \frac{1}{12} b_s E_s h_s^3 \tag{31}$$

$$\rho_2 A_2 = b_s h_s \rho_s \tag{32}$$

REFERENCES

[1] J. Tichy, J. Erhart, E. Kittinger, J. Privratska, 1968, Fundamentals of Piezoelectric Sensorics, Springer-Verlag, Berlin, Heidelberg.

[2] B. Yang Lee, J. Zhang, C. Zueger, Woo-Jae Chung, So Young Yoo, E. Wang, J. Meyer, R. Ramesh and Seung-Wuk Lee, 2012, Virus-based piezoelectric energy generation, Nature Nanotechnology 7, 351:356.

[3] S. R. Anton, and Sodano H. A., A review of power harvesting using piezoelectric materials (2003-2006), 2007, Smart Mater. Struct. 16:R1-R21.

[4] Y. C. Shu and I. C. Lien, 2006, Efficiency of energy conversion for a piezoelectric power harvesting system, J. Micromech. Microeng. 16, 2429Ç:2438

[5] Y.B. Jeon, R. Sood, J. H. Jeong and S. G. and Kim, MEMS power generator with transverse mode thin film PZT, 2005, Sensors Actuators A 122, 16:22

[6] G. Poulin G, E. Sarraute and F. Costa, 2004, Generation of electric energy for portable devices: comparative study of an electromagnetic and a piezoelectric system, Sensors Actuators A 116, 461:71.

[7] S. Roundy, P. K. Wright and J. Rabaey, 2003, A study of low level vibrations as a power source for wireless sensor nodes, Comput. Commun. 26, 1131:1144.

[8] A. Erturk, D. J. Inman, 2001, Piezoelectric Energy Harvesting, Wiley, Chichester, United Kingdom.

[9] H. F. Tiersten, 1969, Linear Piezoelectric Plate Vibrations, Plenum Press, New York.

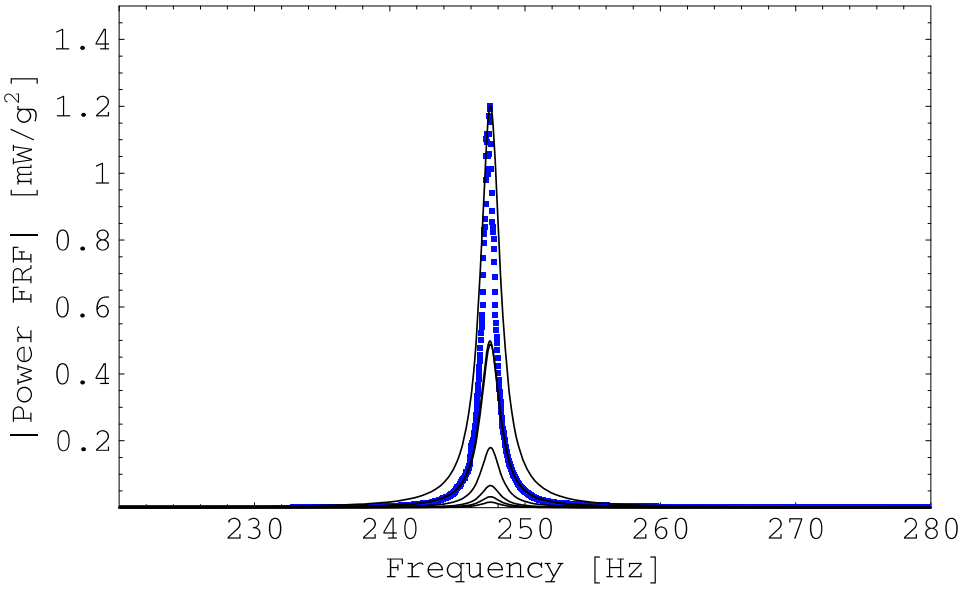

Figure 9: Generated electrical power for frequencies near the second mode of the piezolectric beam of Fig. 8. Solid lines theoretical, circles experimental.

[10] A. Erturk, and D. J. Inman, 2009, An experimentally validated bimorph cantilever model for piezoelectric energy harvesting from base excitations, Smart Mater. Struct. 18, 025009.

[11] S. C. Stanton, C. C. McGehee, B. P. Mann, 2010, Nonlinear dynamics for broadband energy harvesting: Investigation of a bistable piezoelectric inertial generator, Physica D, 239 640:653

[12] J. J. Thomsen, *Vibrations and Stability*, Springer-Verlag, Berlin, (2010).

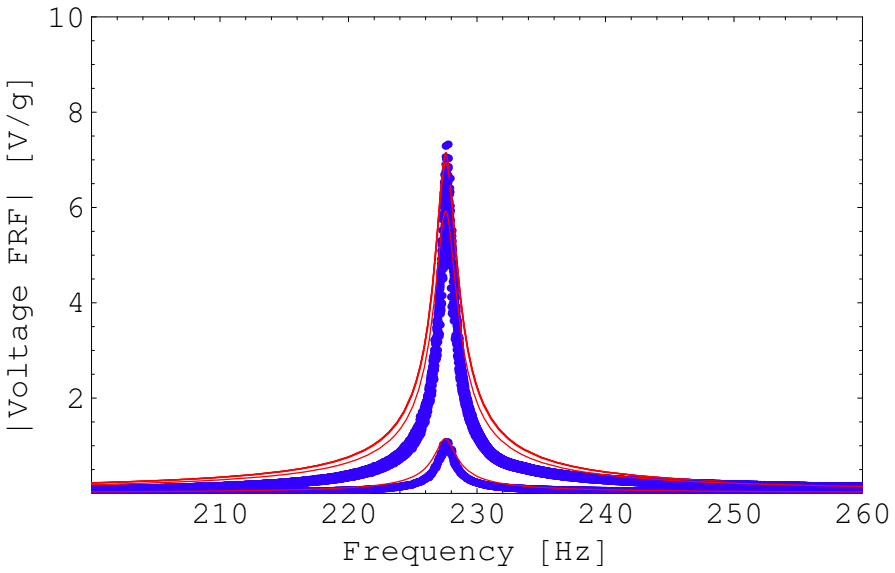

Figure 10: FRFs for frequencies near the second mode of the piezoelectric beam for a given set of resistors. The electromechanical beam has no addition of mass and the system is base-excited. Solid lines theoretical, circles experimental.

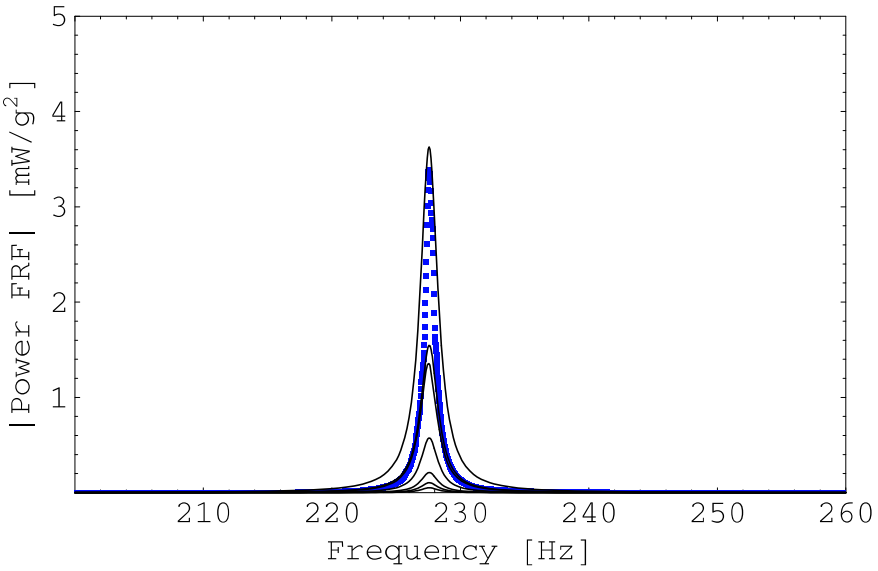

Figure 11: Generated electrical power frequencies near the second mode of the piezoelectric beam of Fig. 10. Solid lines theoretical, circles experimental.

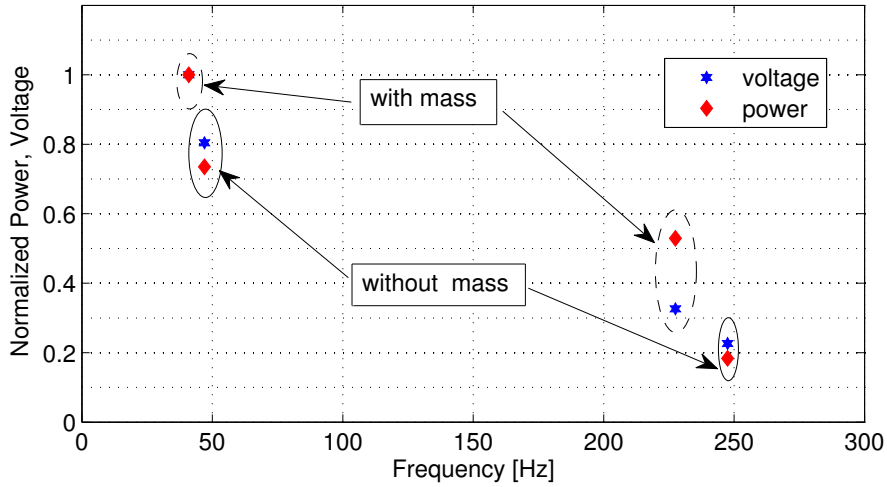

Figure 12: Normalized maximum power and maximum voltage generation comparison as a function of frequency.